ISSN 1330-3651 (Print), ISSN 1848-6339 (Online)
https://doi.org/10.17559/TV-20180622033958
Original scientific paper

Optimization of Slider-Type Hydraulic Powered Support (SHPS) Using FEA and Response Surface Methodology

Yang YANG, Qingliang ZENG, Lirong WAN, Chenglong WANG, Kuidong GAO

Abstract: Optimization design for SHPS is investigated in this paper. Through finite element analysis, SHPS with torsional load on the upper beam and base together is determined as the optimization object. The distance between the cross-section of the live column and the top end of the outer cylinder of the adjustment jack P1, the horizontal distance between axis of lug and rear linkage P2, and the angle P3 of the inclined ramp are chosen as the variable quantity, and the maximum von-Mises stress and maximum total deformation are chosen as evaluation indexes, the size range of each variable is defined in ANSYS WORKBENCH (AW). AW implements force analysis and Solidworks reconstructs the optimization object within the variable range. Two pieces of software jointly implement the continuous modeling and simulation automatically to achieve the 3 factors and 2 levels central composite design experiment of the optimization object. The simulation results after each model reconstruction are recorded in AW. The effects of three selected variables on evaluation indexes are studied and the optimum structure of SHPS is determined. Compared with the original design, the two evaluation indexes decreased by 2,37% and 2,40% respectively, which improves the supporting ability of SHPS efficiently.

Keywords: concentration stress; FEA; model reconstruction; optimization; response surface methodology; slider-type hydraulic powered support

1 INTRODUCTION

Hydraulic powered support is the main supporting equipment for underground mining [1]. As is shown in Fig. 1, the traditional standing shield hydraulic powered support consists of the base 1, leg 2, the front bar 3, the rear bar 4, the shield beam 5, the balance jack 6 and upper beam 7. But for a long time, the traditional hydraulic powered support has the problems of the leg's large inclination angle when working at low position, low working resistance and low supporting efficiency.

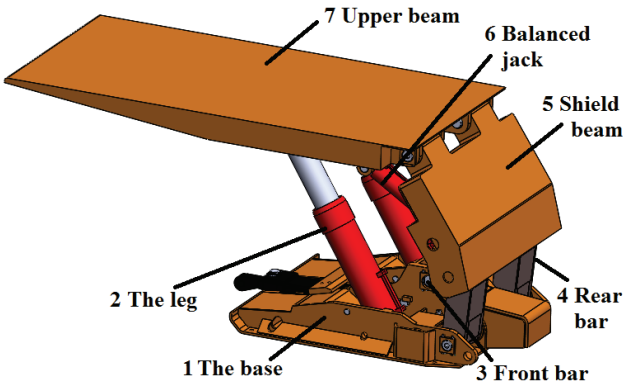

Figure 1 The model of the traditional standing shield hydraulic support

SHPS [2] is a new type hydraulic powered support designed by us which supports the roof by vertical bar 4, slider 3, adjustment jack 2 and inclined ramp 1-a set on the base 1, as is shown in Fig. 2. It is composed of the base 1, the adjustment jack 2, the slider 3, the vertical bar 4, the front bar 5, the rear bar 6, the shield beam 7, the balance jack 8 and upper beam 9. It can effectively improve the supporting efficiency while achieving larger stretching and retracting ratio.

As important underground support equipment, the hydraulic support should have reliable working strength and strong adaptability. In order to study the whole working performance, many scholars have done a lot of research and optimization design to the hydraulic powered support. Oblak et al. [3] proposed a procedure to optimize two groups of parameters of a hydraulic support based on mathematical programming methods.

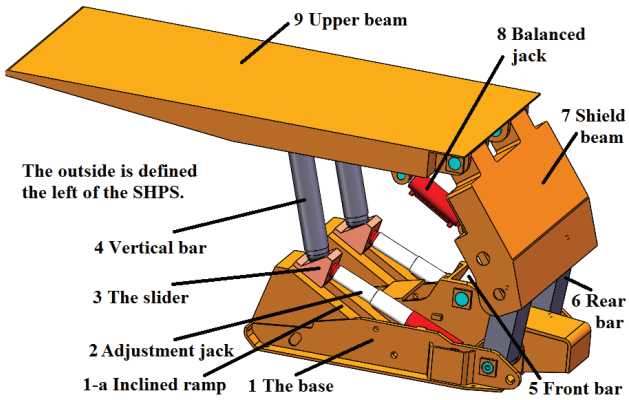

Figure 2 The model of the SHPS

A. K. Verma1 et al. [4] developed the finite element models including the structural components of hydraulic-powered support, the surrounding rock mass and broken rocks to study the interaction between hydraulic support and surrounding rock. Xuewen Wang et al. [5] carried out the force analysis and the stability analysis to the double-telescopic prop of the hydraulic support based on mixed structured and unstructured finite element mesh and buckling analysis method. Xinhua Liu et al. [6] applied numerical simulation on the loaded state of the two-pillar shield-type support based on the inner loading method to research the stress characteristics and deformation law of the high cutting hydraulic support. Marcin Witek et al. [7] put the shield on a hydraulic cushion to simulate the ground with different load-bearing capacities, and the laboratory tests and numerical calculations are carried out to the hydraulic support. Wenshu Cai etal. [8] established the force balance equation of the hydraulic support and carried out the static analysis and modal analysis of the front connecting rod model in MSC Nastran. Tang Mei [13] puts forward a method to improve the structure of the nest through the finite element analysis on the static strength of the nest of the different structure top beam. Guofa Wang et al. [10] use the finite element analysis to optimize and

redesign the structure of the high seam-caving coal hydraulic support based on the coupling model of the surrounding rock and the hydraulic support. Yu et al. [11] studied the dynamic bearing and adaptability of a hydraulic support in a coal caving with a great mining height through theoretical analysis and field monitoring. I. Prebil et al. [12] optimized the four-bar mechanism of hydraulic support through a global optimal solution to find the optimal values of the mechanism link lengths. Dong et al. [13] studied the structure and kinetic characteristic of support by solving plane mechanism equations of a new type of top-coal caving hydraulic support. Xiaohui Zhao et al. [14] applied finite element analysis and fatigue test method to study the fatigue design of the welding structure of powered support. However, people seldom consider the effects of the structure of the hydraulic support on maximum stress and maximum total deformation, which directly influence the maximum support capability of the support, and the structure optimization of the support has not been researched systematically.

With the development of simulation technology, many people have tried to carry out the structure reliability analysis and dynamics analysis by RSM [15]. RSM is a global approximation optimization method, and a design method to study multiple factors level which is often used for structure, materials and performance optimization of equipment, and many researchers have done optimization with this method [16-20]. Therefore, this paper aims at the optimization design for the structure size of SHPS. The distance P1 between the cross-section of the live column and the top end of the outer cylinder of the adjustment jack, the horizontal distance P2 between axis of lug and rear linkage, and the angle P3 of the inclined ramp are chosen as the variable, and the maximum von-Mises stress and maximum total deformation are chosen as optimization object evaluation indexes. The effects of these variables on evaluation indexes are studied and the optimum structure of SHPS is determined by response surface methodology (RSP) which combines the Solidworks model reconstruction and FEA.

The remainder of the paper is organized as follows: Section 2 selects the experimental design method of RSM and constructs the second order response surface model. Section 3 determines the optimization object in SHPS with torsional load on the upper beam and base together by finite element analysis. Section 4 describes the SHPS optimization process using RSM. Section 5 studies the effects of variables on evaluation indexes and the comparison and analysis of the SHPS before and after the optimization is carried out. Section 6 shows some related work and our conclusions.

2 THE SECOND ORDER RESPONSE SURFACE MODEL

The optimization of RSM includes orthogonal design, factorial design, uniform design, central composite design, and D-optimal design. Among them, the distance between the test points and the center points is the same in the central composite design; it has good fitting correlation and predictability and is suitable for the occasion with a few variables. Therefore, the central composite design is chosen for the experimental design in this paper. The second order response surface model [21] can be expressed as:

$$f = k_0 + \sum_{i=1}^{n} k_i x_i + \sum_{i=1}^{n} k_{ii} x_i^2 + \sum_{i=1}^{n} \sum_{j>i}^{n} k_{ij} x_i x_j + \xi \tag{1}$$

The regression coefficient vector $\boldsymbol{k} = [\boldsymbol{k}_1, \boldsymbol{k}_2, ..., \boldsymbol{k}_L]$ can be solved by:

$$\boldsymbol{k} = (\boldsymbol{X}^{\mathrm{T}} \boldsymbol{X})^{-1} \boldsymbol{X}^{\mathrm{T}} f \tag{2}$$

The matrix $\boldsymbol{X}$ consisting of response primary function of design points is:

$$\boldsymbol{X} = \begin{bmatrix} 1 & x_{12} & x_{13} & \cdots & x_{1L} \\ 1 & x_{22} & x_{12} & \cdots & x_{2L} \\ \vdots & & & & \vdots \\ \vdots & & & & \vdots \\ 1 & x_{(S-1)2} & x_{(S-1)3} & \cdots & x_{(S-1)L} \\ 1 & x_{S2} & x_{S3} & \cdots & x_{SL} \end{bmatrix} \tag{3}$$

where f is the response function, x_i, x_j ($i, j = 1, 2, \ldots, n$) are variables, k_0, k_i, k_j ($i, j = 1, 2, \ldots, n$) are regression coefficient, ξ is comprehensive error, L is the number of regression coefficients, S is the number of the test.

3 DETERMINE THE OPTIMIZATION OBJECT BY FEA

The working environment of underground mining is very complex; the contact condition between the hydraulic powered support and the roof or bottom plate, and the load bearing form has great influence on the stability of the support. In order to optimize the support structure so as to reduce the maximum working stress, it is necessary to determine the load bearing state when the maximum stress will occur. According to the Chinese National Standard GB-25974.1-2010 [22], the FEA was used to carry out the simulation of hydraulic support under multiple combined working conditions based on the inner loading method, and the optimization object was determined by the maximum von Mises stress and the maximum total deformation.

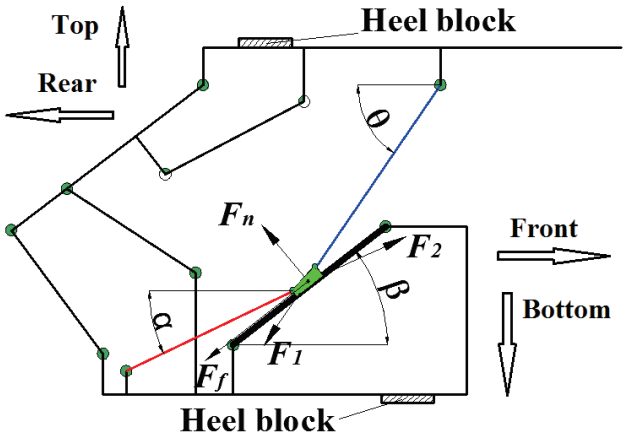

Figure 3 Active braced mechanical bearing model of adjustment jack

3.1 Force Load of the FEA

The working height range of SHPS is 800 ~ 1500 mm and the working resistance is 2100 kN, where the working resistance of SHPS is the supporting force of the vertical bar 4 to the upper beam 9. The SHPS is axisymmetric structure. When the force loading point is located in the middle axis of the upper beam, the force of the vertical bar, the balance jack and the adjustment jack on both sides of the hydraulic powered support are the same.

When the inner loading simulation of SHPS is carried out according to the Chinese National Standard GB-25974,1 - 2010, hydraulic powered support does not bear external force, the adjustment jack is the driving component. The heel block is placed separately on the upper beam and the base according to the working condition. The boundary constraint is applied to the heel block and the constraint type was defined as full constraints to limit the movement of the upper beam and the base. The friction force F_f between the slider and the inclined ramp is upward along the inclined ramp. The mechanical bearing model of SHPS is established and shown in Fig. 3. Total working resistance of two vertical bars to upper beam F_1 = 2100 kN. The static equilibrium equation of the slider is:

$$\begin{cases} F_1 \cdot \sin\theta + F_f \cdot \sin\beta = F_n \cdot \cos\beta + F_2 \cdot \sin\alpha \\ F_1 \cdot \cos\theta + F_n \cdot \sin\beta + F_f \cdot \cos\beta = F_2 \cdot \cos\alpha \end{cases} \tag{4}$$

$$F_2 = \frac{\cos(\beta-\theta) - \mu \cdot \sin(\beta-\theta)}{\cos(\beta-\alpha) - \mu \cdot \sin(\beta-\alpha)} \cdot F_1 \tag{5}$$

$$F_f = \mu \cdot F_n \tag{6}$$

Where F_1 is counterforce from roof to vertical bar, F_n is normal force of the slider, F_2 is total driving force of two adjustment jacks, μ is the friction coefficient between steel and steel, α is dip angle of adjustment jack, β is dip angle of inclined ramp, θ is dip angle of vertical bar.

According to the Chinese National Standard GB-25974.1-2010, the working height of the SHPS is 1100 mm when the inner loading test under the condition of the eccentric load on the upper beam is carried out on the SHPS, α, β, θ is 18,4°; 30°; 45,3° respectively, F_2 is 2221 kN, the driving force of every adjustment jack F_{2s} is 1110,5 kN. The working height of the SHPS is 1266,7 mm when the inner loading test is carried out under other condition, α, β, θ is 20,6°; 30°; 56,5° respectively, F_2 is 2099,5 kN, the driving force of every adjustment jack F_{2s} is 1049,75 kN.

3.2 FEA to SHPS

Establish the 3D models of SHPS at the height of 1100 mm and 1266,7 mm by Solidworks. Chamfers and other structures of SHPS with no effect on its strength was rationally simplified. A section of the live column and the bottom of the outer cylinder were respectively arranged at the column nest of the slider and the lug set on the base. Position and size of the heel block are established according to Chinese National Standard GB-25974.1-2010, as is shown in Fig. 4.

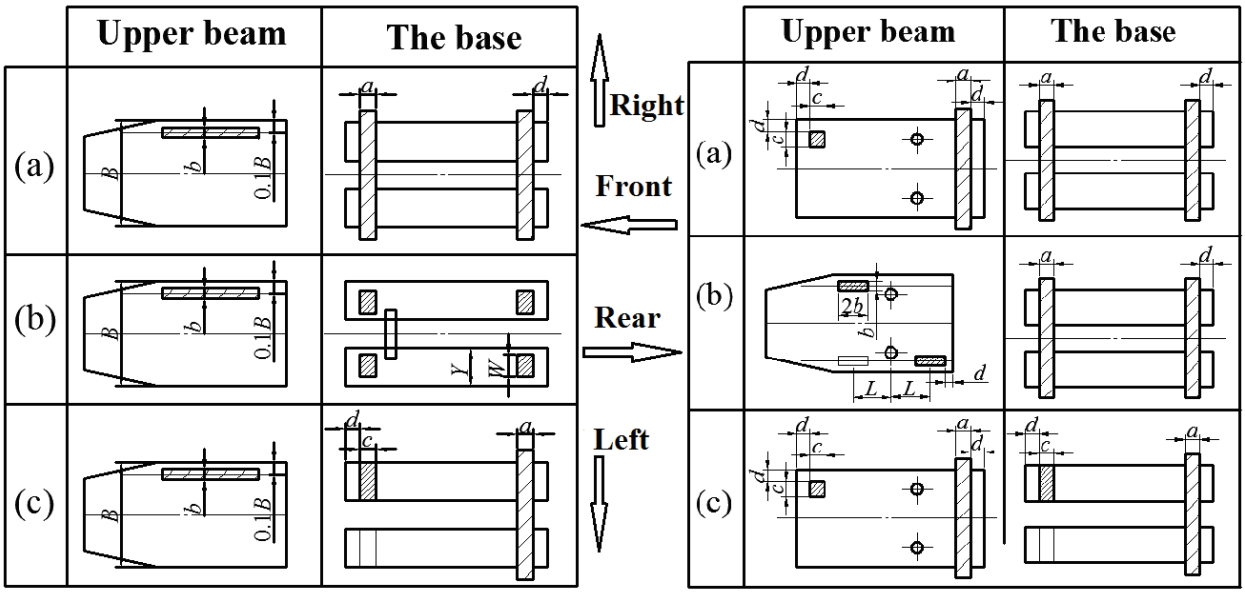

(1) (2)

Figure 4 Position and size of heel block. (1) Upper beam bearing the eccentric load; (2) Other test conditions

Position and size of heel blocks under conditions of load combined by eccentric load on the upper beam and load on both ends of the base, eccentric load on the upper beam and load on four corners of the base, eccentric load on the top beam and torsion load on the base are shown in Fig. 4(1)-(a), Fig. 4(1)-(b) and Fig. 4(1)-(c), the working height of SHPS is 1100 mm under three conditions.

Position and size of heel blocks under conditions of load combined by torsion load on the upper beam and load on both ends of the base, load on the diagonal corners of the upper beam and load on both ends of the base, torsion load on the upper beam and torsion load on the base are shown in Fig. 4(2)-(a), Fig. 4(2)-(b) and Fig. 4(2)-(c), and the working height of SHPS is 1266,7 mm. The sizes of Fig. 4 are: a = 150 mm; b = 200 mm; c = 300 mm; d = 50 mm; B = 1440 mm; Y = 328 mm; $W = Y - 100$; thickness of heel blocks h = 50 mm.

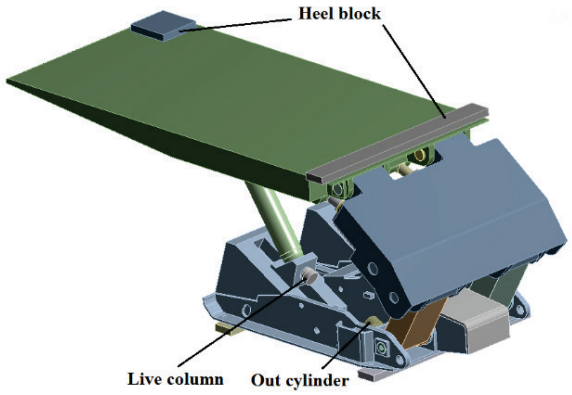

Figure 5 Example of FEA model of the SHPS

Importing the 3D model into AW is shown in Fig. 5. The material properties of components, connection relation and friction are defined. The constraints are applied to the heel blocks respectively and the type of the constraint is "fully constraint". In order to calculate accurately, Hex dominant method is used to divide the mesh of the SHPS.

According to the Chinese National Standard GB-25974.1-2010, the safety factor of non-column nest loading test s = 1,2. Surface load p_1 and p_2 are applied on the across sections of live column and the bottom of the outer cylinder separately. The surface loads are calculated by:

Upper beam bearing the eccentric load:

$$p_1 = \frac{1,2F_{2s}}{S_1} = 169,76 \text{ MPa} \tag{6}$$

$$p_2 = \frac{1,2F_{2s}}{S_2} = 117,89 \text{ MPa} \tag{7}$$

Other test conditions:

$$p_1 = \frac{1,2F_{2s}}{S_1} = 160,48 \text{ MPa} \tag{8}$$

$$p_2 = \frac{1,2F_{2s}}{S_2} = 111,44 \text{ MPa} \tag{9}$$

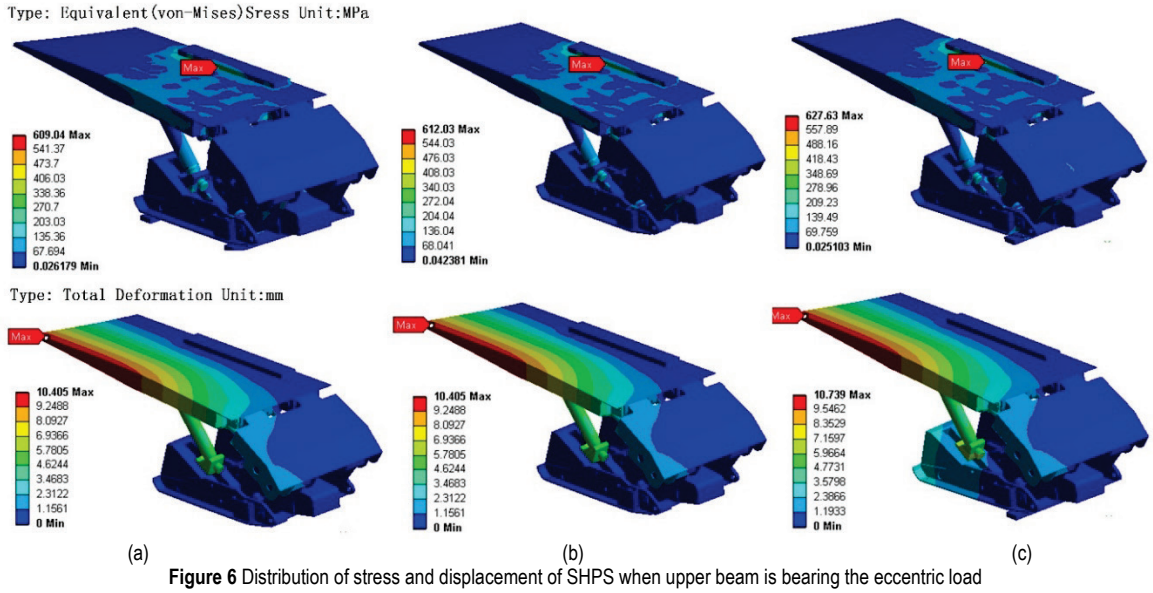

Figure 6 Distribution of stress and displacement of SHPS when upper beam is bearing the eccentric load

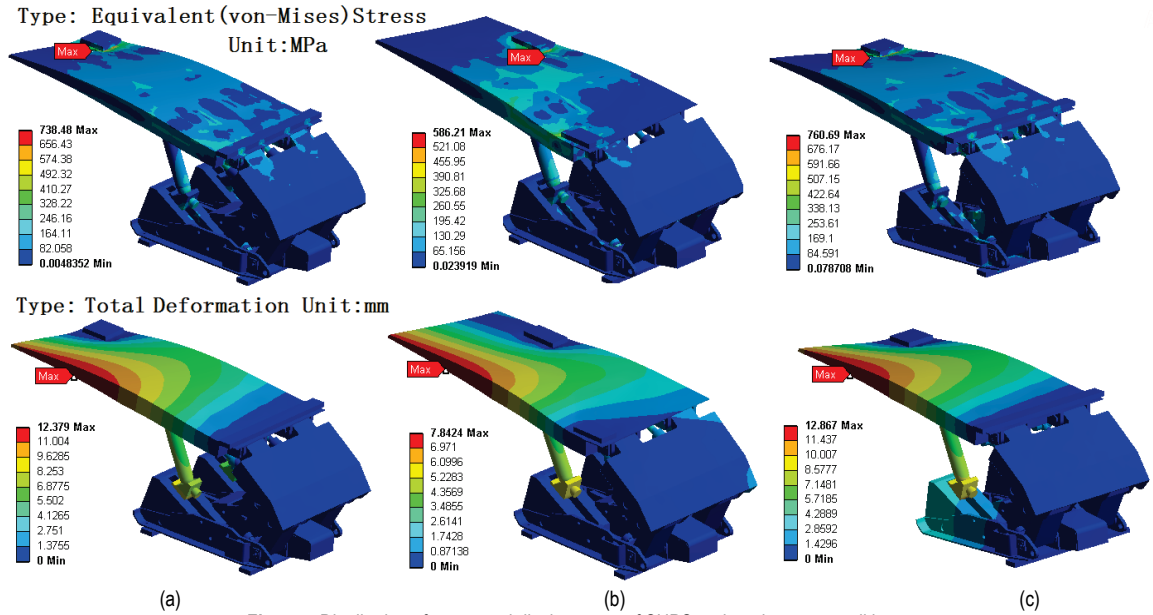

Figure 7 Distribution of stress and displacement of SHPS under other test conditions

3.3 Determine the Optimization Object

The distribution of stress and displacement of SHPS under conditions of load combined by eccentric load on the upper beam and load on both ends of the base, eccentric load on the upper beam and load on four corners of the base, eccentric load on the top beam and torsion load on the base are shown as Fig. 6(a), Fig. 6(b), Fig. 6(c) separately, where the stress is von Mises stress and the unit is MPa, the unit of displacement is mm.

According to Fig. 6, the maximum von Mises stress at the bottom of the heel block and near the column nest of the upper beam under three kinds of loading modes while the upper beam is bearing the eccentric load, and the maximum total deformation appears at the front end of the upper beam away from the side where the heel block is located. The differences between the values of maximum von Mises stress and displacement under different working conditions are few. Under condition of load combined by an eccentric load on the top beam and torsion load on the base, the maximum von Mises stress and displacement are relatively larger and are up to 627,63 MPa and 10,74 mm.

The distribution of stress and displacement of SHPS under conditions of load combined by torsion load on the upper beam and load on both ends of the base, load on the diagonal corners of the upper beam and load on both ends of the base, torsion load on the upper beam and base together are shown as Fig. 7(a), Fig. 7(b), Fig. 7(c) separately, where the stress is von Mises stress and the unit is MPa, the unit of displacement is mm.

According to Fig. 7, the maximum von Mises stress is also near the heel block but far away from the column nest under three kinds of other test conditions while the upper beam bearing the eccentric load, and the maximum total deformation also appear at the front end of the upper beam away from the side where the heel block is located. The maximum von Mises stress and displacement under condition of torsion load both on the top beam and on the base are larger in the three other test conditions which are up to 760,69 MPa and 12,87 mm.

Comparing the six groups of inner loading simulation results, when the upper beam is bearing the torsion load, the maximum stress of SHPS is more than 730 MPa and the maximum total deformation is above 12 mm. Therefore, the torsion load on the upper beam should be avoided as far as possible in the working process of the SHPS. The SHPS under condition of torsion load both on the top beam and on the base has the largest maximum von Mises stress and maximum total deformation, this condition is the worst working condition for the SHPS, so the SHPS under condition of torsion load both on the top beam and on the base is selected as the optimization object.

4 OPTIMIZATION BY RSM

The response surface methodology was used to optimize the SHPS under the condition of torsion load both on the upper beam and the base. During the optimization process of this article, AW implements the force analysis of the model, Solidworks software reconstructs the model within the range of variable values. AW and Solidworks jointly implement the continuous modeling and simulation within the design variable range of the SHPS automatically under the condition of torsion load both on the upper beam and the base and record the value of the evaluation index after each simulation.

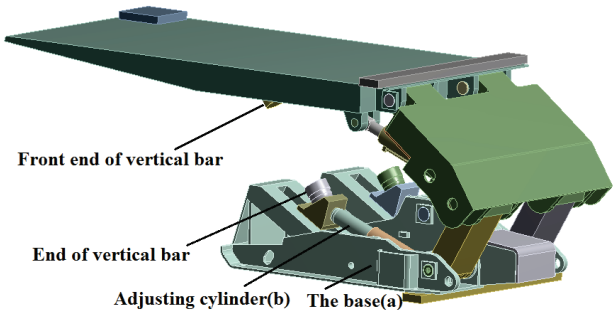

Figure 8 The optimization model of the SHPS

After the interface set between AW and Solidworks, the 3D model of the optimized object is established in Solidworks software. The heel block at the upper beam and the base is established according to Fig. 4-2(c). In the optimization process, the variable changes will alter the position of the vertical bar and the adjustment jack so as to change the force on the adjustment jack. The methods that cancel the structure of the adjustment jack according to Fig. 5 and apply the surface force p_1, p_2 to the live column and bottom of the outer cylinder in accordance with Eq. (5) and Eq. (6) cannot guarantee the constant force of the vertical bar. Therefore, when we build the 3D model, retaining the adjustment jack, canceling the structure of the vertical bar, and retaining only a section of tip and tail of the vertical bar, then the surface force can be applied to the section of the vertical bar directly during simulation. The 3D model of the optimized object is shown in Fig. 8.

After the 3D model is established, the AW program is invoked in Solidworks software to set up the optimization system. The material parameters of each component and the connection relationship between the components are defined in WORKBENCH, friction is added, and the constraint which is full restraint is imposed on the heel block at the upper beam and the base.

The surface force p_3 is applied at the tip and tail of the vertical bar respectively:

$$p_3 = \frac{1,2F_{2s}}{S_3} = 71,3375 \text{ MPa} \tag{10}$$

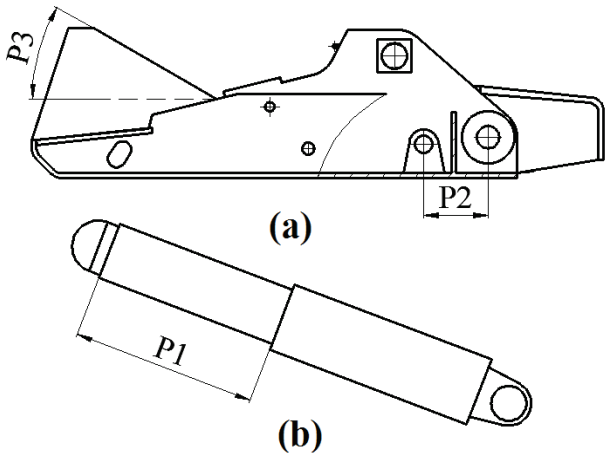

Figure 9 Variable parameters of the SHPS

To simplify the calculation, the double telescopic adjustment jack is transformed to a single telescopic adjustment jack with the same length. Meanwhile, taking the distance between the cross-section of the live column and the top end of the outer cylinder of the adjustment jack P1, the horizontal distance between axis of lug and rear linkage P2, and the angle P3 of the inclined ramp as the design variables, the dimensions of other structures of the SHPS remain unchanged as shown in Fig. 9. Define the size ranges of each variable in AW. The maximum von-Mises stress of P4 and the maximum total deformation of P5 were taken as the evaluation indicators. Conducted 3 factors and 2 levels central composite design after other related settings are performed, and some experimental results are listed in Tab. 1.

Table 1 Some experimental results

Node	P1 / mm	P2 / mm	P3 / °	P4 / MPa	P5 / mm
1	284,464	220	30	638,608	11,384
2	264,464	220	30	641,359	11,321
3	304,464	220	30	989,133	10,073
4	284,464	200	30	653,338	11,316
5	284,464	240	30	644,092	11,489
6	284,464	220	26	650,582	11,601
7	284,464	220	34	626,526	11,174
8	268,204	203,74	26,748	641,973	11,435
9	300,725	203,74	26,748	647,786	11,576
10	268,204	236,26	26,748	647,598	11,554
11	300,725	236,26	26,748	1000,488	10,270
12	268,204	203,74	33,252	630,410	11,110
13	300,725	203,74	33,252	635,949	11,223
14	268,204	236,26	33,252	696,669	11,208
15	300,725	236,26	33,252	959,375	9,939

5 ANALYSIS AND DISCUSSION OF OPTIMIZATION RESULTS

5.1 Response Relationship between Design Variables and Evaluation Indexes

After the optimization using RSM, we get the sensitivity of the design variables P1, P2, and P3 to the maximum von-Mises stress of P4 and maximum total deformation of P5, which are shown in Fig. 10.

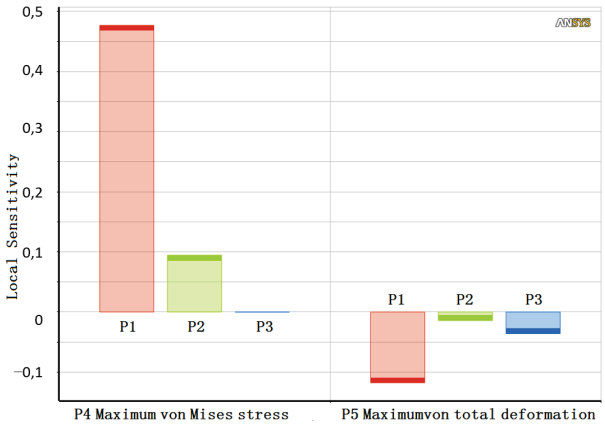

Figure 10 The sensitivity of design variables to target variables

Fig. 10 shows that the sensitivity of P1, P2 to P4 is great, and the value of P3 has little effect on P4. For the maximum total deformation of P5, P1 has the greatest sensitivity to the influence on it and is followed by P3, P2 which has the least effect on it. Owing to less fluctuation of the maximum total deformation value, the purpose of the structural optimization is to change the overall stress state of the SHPS. Therefore the influence of each variable on the maximum stress value is emphatically considered.

Ignoring the effect of P3 on P4, take P3 as a constant value, the curved surface response diagram between the variable P1, P2 and the maximum stress of P4 is shown in Fig. 11. The response relationships of single variable P1 and P2 to the maximum stress of P4 are shown in Fig. 12 separately.

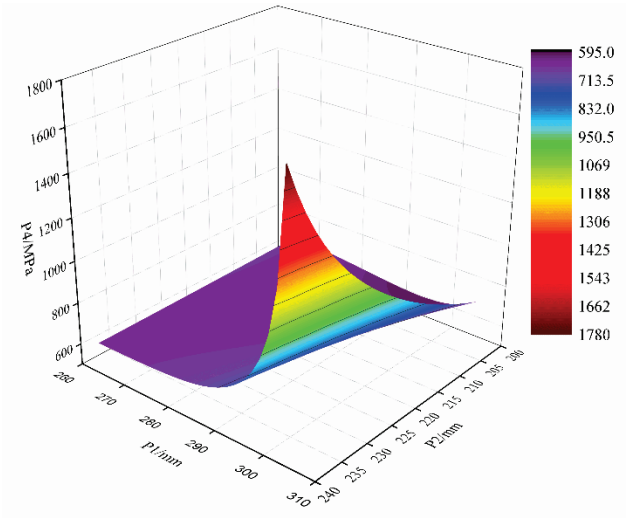

Figure 11 Surface response diagram between P1, P2 and P4

The curved surface response diagram in Fig. 11 shows the tendency of both ends to be high and concave in the middle. The maximum von-Mises stresses P4 changes slowly when P1 and P2 are small. The maximum von-Mises stresses P4 increases sharply with the increase of P1 and P2 when P1 and P2 are large, and the largest maximum von-Mises stress P4 occurs at the maximum value of P1 and P2.

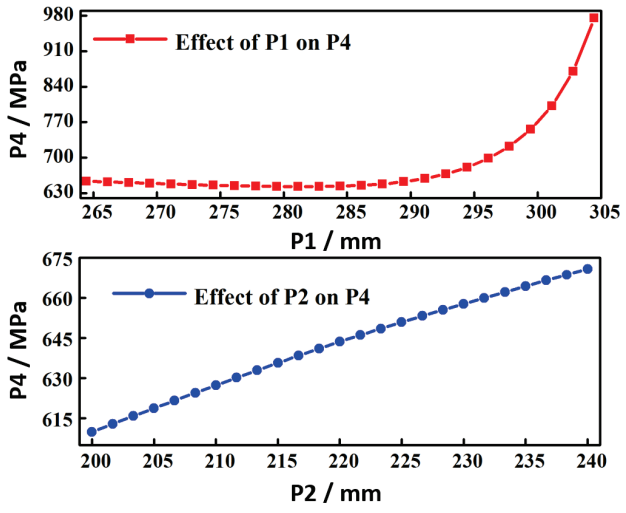

Figure 12 The relationship between individual variable and P4

As is shown in Fig. 12, the maximum von Mises stress P4 shows the tendency that decreases first and then increases with the increase of P1 when P2 and P3 take fixed values. The minimum point of P4 appears in the position when P1 is 284,5 mm. When P1 is greater than 284,5 mm, P4 increases rapidly with the increase of P1. When P1 and

P3 are fixed, P4 increases gradually with the increase of P2, and the growth rate is small.

Therefore, when the inclined angle P3 is determined, P1 has a great influence on the force of the SHPS. In the process of designing the SHPS, for the SHPS with a height of 1266,7 mm, the length of P1 is near the value of 284,5 mm which can improve the structure force of the hydraulic powered support effectively, and P2 should select the minimum value within its allowable range.

5.2 Determination of Optimal Structure of SHPS

The ultimate stress and displacement values obtained by RSM are listed in Tab. 2. When P5 is 8,966 mm and 9,422 mm, P4 is 1776,155 MPa which does not meet the optimization requirements. While P1 is 292,994 mm, P2 is 200 mm, P3 is 29,2°, and the maximum von Mises stress P4 gets a minimum value of 595,739 MPa while P5 is only 11,696 mm. The result is in accordance with the rule shown in the curved surface response diagram in Fig. 11.

The optimized model of SHPS was determined according to the optimized data. The length of the vertical bar changed from 790 mm before optimization to 802,211 mm due to the change of the three optimization variables. When the optimized model of the SHPS is at the height of 1266,7 mm, the angles α, β and θ are 19,636°; 29,2°, and 56,515° respectively.

Table 2 The ultimate stress and displacement values obtained by RSM

Limit point	P1 / mm	P2 / mm	P3 / °	P4 / MPa	P5 / mm
Minimum von Mises Stress	292,994	200	29,200	595,739	11,696
Maximum von Mises Stress	304,464	240	34	1776,155	8,966
Minimum Total Deformation	304,464	240	26,666	1776,155	9,422
Maximum Total Deformation	295,028	200	26	597,127	11,874

5.3 Analysis of the Optimization Results

According to the position relationship of the SHPS after the structure is optimized, the adjustment jack F_2 = 2091,59 kN when the vertical bar F_1 = 2100 kN. During the simulation, each adjustment jack force $F'_2 = s \cdot F_{2S}$ = 1254,95 kN. Then we establish the 3D model of the SHPS, among them the heel block at the upper beam and the base are established according to Fig 4(2)-(c). Retaining the vertical bar, canceling the adjustment jack, and retaining a section of the tip and tail of the adjustment jack during the process of modeling. And then importing the 3D model into WORKBENCH to define the material parameters, divide the mesh, apply full constraints on the heel block and apply surface forces p'_1, p'_2 on the sections of the active column and bottom of the cylinder. The FEA is carried out to the structure optimized SHPS under the condition of torsion load both on the upper beam and the base.

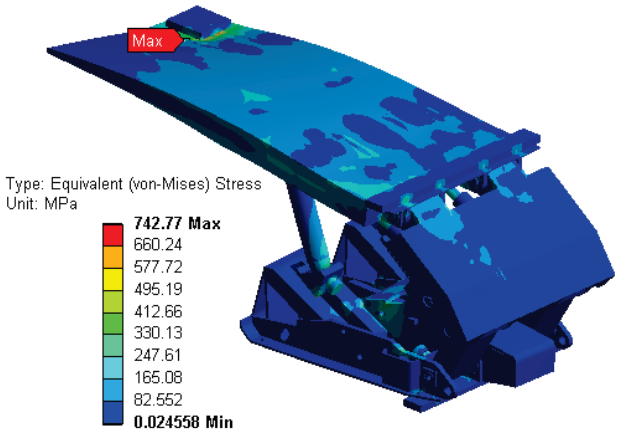

Figure 13 Distribution of stress after optimization

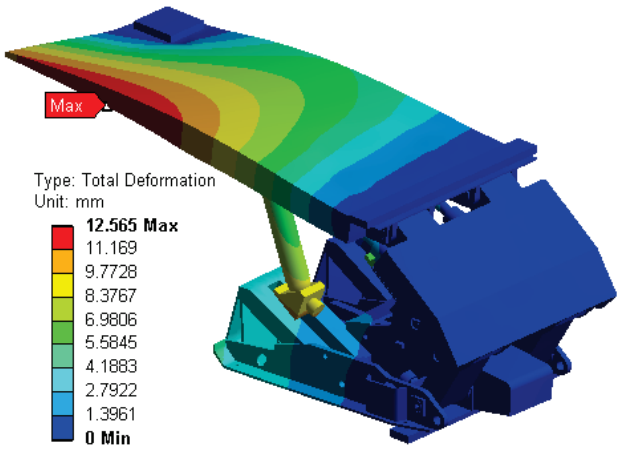

Figure 14 Distribution of displacement after optimization

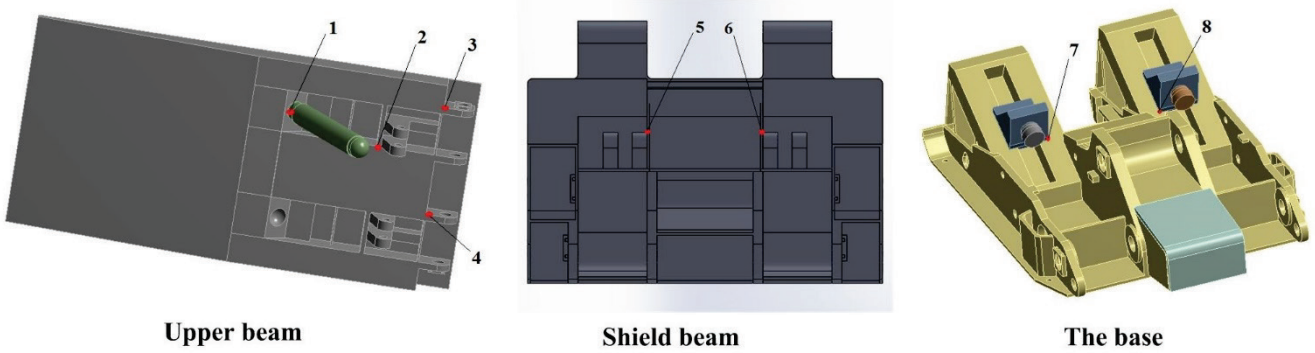

Figure 15 The positions of the stress concentration points

The distribution of stress and displacement are shown in Fig. 13 and Fig. 14 which are obtained from the FEA of the SHPS. Meanwhile, the maximum von Mises stress of the SHPS is 742,77 MPa and the maximum total deformation is 12,565 mm, and the position of the maximum von Mises stress and the maximum total

deformation is the same as Fig. 7(c). The maximum von Mises stress and maximum total deformation are reduced by 2,40% and 2,37% respectively after optimization.

Table 3 Point stress before and after optimization

Stress Point	Stress before Optimization	Stress after Optimization	Percentage Reduction
Point1	488,59	476,23	2,53
Point2	444,32	408,22	8,12
Point3	441,88	434,44	1,68
Point4	387,19	377,37	2,54
Point5	329,24	300,41	8,76
Point6	384,98	288,30	25,11
Point7	657,96	612,13	6,97
Point8	267,06	239,79	10,21

Under the working condition of the torsion load on the upper beam and base together, the stress concentration appears many times on the upper beam, the vertical bar, the shield beam and the slider of the SHPS. The larger stress point is marked and their position coordinates are shown in Fig. 15. The von Mises stress values of the stress concentration points in Fig. 7(c) and Fig. 13 were extracted, and the results are shown in Tab. 3 and Fig. 16.

It can be seen from Tab. 3 and Fig. 16 that the concentration stress at the upper beam, the shield beam, the vertical bar and others are significantly reduced after the SHPS optimization, and the values vary from 1,68% to 25,11%.

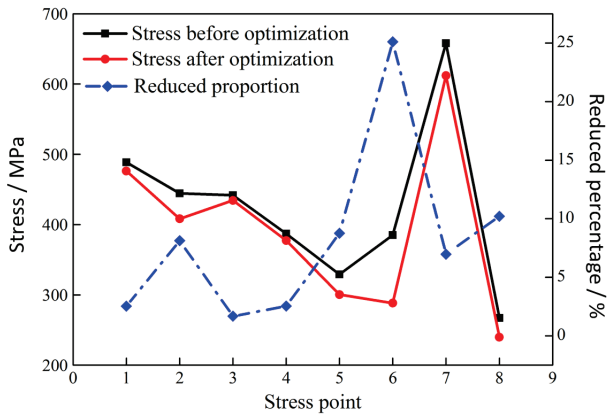

Figure 16 Point stress and stress reduced proportion

Concentrated stress of the shield beam has been greatly reduced, and the stress reduced ratio is up to 25,11%. Maximum concentration stress reduced ratio of the slider is more than 10%. The reduction of the stress value at the stress concentration point reduces the requirement of the slider on its own material strength and improves the working reliability.

While the upper beam has the smallest change of stress, the reduction ratio of stress ranges from 1,68% to 8,12% after optimization. The reason is that the vertical bar supports the upper beam directly and the working resistance remains constant, while the inclined angle of the vertical bar changes little. So that the changing degree of the force transmitted via the vertical bar to the upper beam is small. Although the stress reduction proportion is smaller than before optimization, it can effectively improve the adaptability of the hydraulic support to the roof, meet the requirement of working intensity and provide greater bracing force as well.

6 CONCLUSIONS

To reduce the ultimate stress when the SHPS is working, a response surface methodology is carried out to optimize the parameters based on the FEA results of the support under multiple loading conditions. The effects of these parameters on evaluation indexes and optimization results are investigated. The following conclusions can be drawn from the results obtained in this study:

The SHPS under the condition of torsion load both on the upper beam and the base has the maximum von Mises stress of 760,69 MPa and the maximum total deformation of 12,87 mm, which is the worst working condition of the SHPS. And it is the SHPS under this condition that is considered as the optimization object. After optimization, the maximum von Mises stress and maximum total deformation of the SHPS were reduced by 2,40% and 2,37% under the same conditions. The maximum concentration stress reduction ratio of the shield beam was up to 25%, and the maximum concentrated stress of the slider was reduced by more than 10%. The optimized stress reduction ratio of upper beam was 1,68% ~ 8,12%, and the overall supporting strength of the SHPS was improved.

P1 and P2 are more sensitive to the maximum stress value of P4, while the value of P3 has almost no effect on P4. P1 has the greatest sensitivity to the maximum total deformation of P5. P2 has the smallest influence on P4. When the height of the SHPS is 1266,7 mm, the length of P1 is near the value of 284,5 mm which can improve the structure force of the SHPS effectively, P2 should select the minimum value within its allowable range. And it is better for the upper beam to avoid the torsion load when the SHPS is in the application

Acknowledgements

This work was supported by National Natural Science Foundation of China (No. 51674155), Innovative Team Development Project of Ministry of Education (Grant No. IRT_16R45), Natural Science Foundation of Shandong Province (Grant No. ZR2016EEM09), Major Research and Development Projects of Shandong Province (Grant No. 2018GGX103027).

7 REFERENCES

[1] Yang, Y., Zeng, Q. L., Zhou, J. H., Wan, L. R., & Gao, K. D. (2018). The design and analysis of a new slipper-type hydraulic support. *Plos one*, *13*(8), 1-22. https://doi.org/10.1371/journal.pone.0202431

[2] Zeng, Q. L.,Yang, Y., Meng, Z. S., Kong, S.,Wan, L. R., & Li, Y. L. (2017). Kinematics Characteristics Analysis of New Hexaglide Hydraulic Support for Thin Coal Seam. *Coal Technology*, *36*(2), 214 216.

[3] Oblak, M., Harl, B., & Butinar, B. (2014). Optimal design of hydraulic support. *Struct Multidisc Optim*, *20*, 76-82. https://doi.org/10.1007/s001580050138

[4] Verma, A. K. & Deb, D. (2013). Numerical Analysis of an Interaction between Hydraulic-Powered Support and Surrounding Rock Strata. *International Journal of Geomechanics*, *13*(2), 181-192. https://doi.org/10.1061/(ASCE)GM.1943-5622.0000190

[5] Wang, X. W., Yang, Z. J., Feng, J. L., & Liu, H. J. (2013). Stress analysis and stability analysis on doubly-telescopic

prop of hydraulic support. *Engineering Failure Analysis*, 32, 274-282. https://doi.org/10.1016/j.engfailanal.2013.04.006
[6] Liu, X. H., Wang, G. F., & Liu, C. F. (2010). Full Set Finite Element Analysis on Two-Leg High Cutting Hydraulic Powered Support. *Coal Science and Technology*, *38*(8), 93-96.
[7] Marcin, W. & Stanisław, P. (2016). Numerical calculations of shield support stress based on laboratory test results. *Computers and Geotechnics*, 72, 74-88. https://doi.org/10.1016/j.compgeo.2015.11.007
[8] Cai, W. S., Cheng, Z. H., Shen, C. F., & Song, Y. P. (2009). Finite Element Analysis on Front Link of Hydraulic Powered Support. *Coal Science and Technology*, *37*(4), 69-71.
[9] Tang, M. (2013). Finite Element Analysis for Nest of Shield. *Journal of Shanghai Electric Machinery College*, 1, 20-24.
[10] Wang, G. F., Liu, J. F., & Ren, H. W. (2011). Design and optimization of high seam-caving coal hydraulic support based on model of support and wall rock coupling. *Journal of China Coal Society*, *336*(1), 145-151.
[11] Yu, L., Yan, S. H., Yu, H. Y., & Zhang, Z. (2011). Studying of dynamic bear characteristics and adaptability of support in top coal caving with great mining height. *Procedia Engineering*, 640-646. https://doi.org/10.1016/j.proeng.2011.11.2217
[12] Prebil, I., Kragna, S., & Ciglarie, I. (2002). Synthesis of four-bar mechanism in a hydraulic support using a global optimization algorithm. *Industrial applications and design case studies*, 246-251. https://doi.org/10.1007/s00158-002-0234-y
[13] Dong, Z., Tang, Y. J., Liu, J. H., Wu, H. X., Zhou, Y. Q., & Wu, J. (2004). Mechanisms and Virtual Design of a New Type of Top-Coal Caving Hydraulic Support. *Proceedings of the 11th World Congress in Mechanism and Machine Science*. Tianjin: China Machine Press. https://doi.org/10.3901/CJME.2004.supp.205
[14] Zhao, X. H., Li, F. Y., Liu, Y., & Fan, Y. J. (2015). Fatigue Behavior of a Box-Type Welded Structure of Hydraulic Support Used in Coal Mine. *Materials*, 8, 6609-6622. https://doi.org/10.3390/ma8105325
[15] Xie, J., Zhao, S. D., Liang, J. T., & Ma, H. K. (2012). Variable Sequential Combination Response Surface Methodology for Press Rod System Optimization. *Journal of Xi'an Jiaotong University*, *46*(5), 57-62.
[16] Hussan, M., Rahman, M. S., Sharmin, F., Kim, D., & Do, J. (2018). Multiple tuned mass damper for multi-mode vibration reduction of offshore wind turbine under seismic excitation. *Ocean Engineering*, 160, 449-460. https://doi.org/10.1016/j.oceaneng.2018.04.041
[17] Box, G. E. P. & Draper, N.R. (2007). *Response Surfaces, Mixtures, and Ridge Analysis, second ed*. John Wiley & Sons, Inc, Hoboken, New Jersey, USA. https://doi.org/10.1002/0470072768
[18] Kim, D., Khan, A., & Do, J. (2016). Cost effective optimal mix proportioning of high strength self-compacting concrete using response surface methodology. *Computers & Concrete*, *17*(5), 629-648. https://doi.org/10.12989/cac.2016.17.5.629
[19] Khan, A., Do, J., & Kim, D. (2006). Experimental optimization of high-strength self-compacting concrete based on D-optimal design. *Journal of Construction Engineering & Management*, *143*(4), 433-440. https://doi.org/10.1061/(ASCE)CO.1943-7862.0001230
[20] Luo, D., Feng, Z. X., & Wang, X. Y. (2012). Parameter optimization for compacting system of asphalt paver based on response surface method. *Journal of Vibration and Shock*, *31*(15), 92-95+100.
[21] Bahloul, A., Mhalla, M. M., & Bouraoui, C. (2018). Crack repair of SENT specimen using the interference fit process. *Journal of Alloys and Compounds*, 748, 363-374. https://doi.org/10.1016/j.jallcom.2018.03.142
[22] China Coal Industry Association. (2011). *Powered Support for Coal Mine-Part 1: General Specification*. Standardization Administration of the People's Republic of China, Beijing, China

Contact information:

Yang YANG, PhD, candidate student,
College of Mechanical and Electronic Engineering,
Shandong University of Science and Technology,
266590 Qingdao, China
E-mail: yang.yang@sdust.edu.cn,
sdkdyangyang@126.com

Qingliang ZENG, Prof. Dr.
(Corresponding author)
College of Mechanical and Electronic Engineering,
Shandong University of Science and Technology,
266590 Qingdao, China
E-mail: qlzeng@sdust.edu.cn

Lirong WAN, Prof. Dr.
College of Mechanical and Electronic Engineering,
Shandong University of Science and Technology,
266590 Qingdao, China
E-mail: lirong.wan@sdust.edu.cn

Chenglong WANG, Associate Prof. Dr.
College of Mechanical and Electronic Engineering,
Shandong University of Science and Technology,
266590 Qingdao, China
E-mail: wclcm@sdust.edu.cn

Kuidong GAO, Associate Prof. Dr.
College of Mechanical and Electronic Engineering,
Shandong University of Science and Technology,
266590 Qingdao, China
E-mail: gaokuidong22@163.com

Appendix: List of used symbols and their SI units

Symbols	Meaning	SI units
f	Response function	--
k_0, k_i, k_j	Regression coefficient	--
ξ	Comprehensive error	--
L	Number of regression coefficient	--
S	Number of the test	--
F_1	Counterforce from roof to vertical bar	kN
F_n	Normal force of the slider	kN
F_2	Total driving force of two adjustment jack	kN
F_f	Friction force between the slider and the inclined ramp	kN
μ	Friction coefficient between steel and steel	
α	Dip angle of adjustment jack	°
β	Dip angle of inclined ramp	°
θ	Dip angle of vertical bar	°
p_1, p_2	Surface load applied on the across sections of live column and the bottom of the outer cylinder	MPa
p_3	Surface force applied at the tip and tail of the vertical bar	MPa
P1	Distance between the cross-section of the live column and the top end of the outer cylinder of the adjustment jack	mm
P2	Horizontal distance between axis of lug and rear linkage	mm
P3	Angle of the inclined ramp	°
P4	Maximum von-Mises stress	MPa
P5	Maximum total deformation	mm